Murtada, S.; Latorre, M.; Humphrey, JD. (2022). Remodeling of the uterine artery during and early after pregnancy in the mouse. Biomechanics and Modeling in Mechanobiology. 22:1531-1540. https://doi.org/10.1007/s10237-022-01674-2

Remodeling of the Uterine Artery During and Early After Pregnancy in the Mouse

Sae-Il Murtada[1,*], Marcos Latorre[2,*], Jay D. Humphrey[1,3]

[1]Department of Biomedical Engineering
Yale University, New Haven, CT, USA

[2] Center for Research and Innovation in Bioengineering
Universitat Politècnica de València, València, Spain

[3]Vascular Biology and Therapeutics Program
Yale School of Medicine, New Haven, CT, USA

[*]These authors contributed equally

Address for Correspondence: jay.humphrey@yale.edu

ORCID 0000-0003-1011-2025

ACKNOWLEDGMENTS

This work was made possible by discretionary funds provided by Yale University.

ABSTRACT

Pregnancy associates with dramatic changes in maternal cardiovascular physiology that ensure that the utero-placental circulation can support the developing fetus. Particularly important is the marked flow-induced remodeling of uterine arteries during pregnancy and their recovery following delivery. Whereas details are available in the literature on alterations in hemodynamics within and changes in the dimensions of uterine arteries during and following pregnancy in mice, we report here the first biaxial biomechanical phenotyping of these arteries during this dynamic period of growth and remodeling (G&R). To gain additional insight into the measured G&R, we also use a constrained mixture model to describe and predict findings, including simulations related to fetal growth restriction. It is found that pregnancy-induced remodeling of the uterine artery is largely, but not completely, reversed in the postpartum period, which appears to be driven by dramatic increases in collagen turnover among other intramural changes. By contrast, data on the remodeling of the ascending aorta, an elastic artery, reveal modest changes that are fully recovered post-partum. There is strong motivation to continue biomechanical studies on this critical aspect of women's health, which has heretofore not received appropriate consideration from the biomechanics community.

Keywords: uterine artery, adaptation, pregnancy, antepartum, postpartum

INTRODUCTION

Arteries typically exhibit a remarkable ability to adapt to modest changes in blood flow and pressure according to mechanobiological principles. If, for example, we let ε denote a sustained fold-change in blood flow and γ a sustained fold-change in blood pressure, then changes in luminal radius a and wall thickness h tend to follow specific rules that restore flow-induced mean wall shear stress and pressure-induced mean circumferential wall stress toward original (homeostatic) values, namely (Humphrey, 2008): $a \rightarrow \varepsilon^{1/3} a_o$ and $h \rightarrow \varepsilon^{1/3} \gamma h_o$ where $a_o$and h_o denote original homeostatic values. These changes typically associate with compositional changes that can alter intrinsic material properties, such as material stiffness and elastic energy storage, and structural properties that are reflected by pulse wave velocity (PWV) or the so-called distensibility D. Importantly, however, such adapted values need not revert back fully to original values upon reversal of a perturbation. As an example, it was reported long ago that the expected thickening of the wall of the aorta during hypertension did not reverse fully when blood pressure was returned toward normal for an extended period, an observation that was sex dependent (Wolinsky, 1971). It has also been shown that when stretched axially *in vivo*, arteries tend to grow longer to restore the axial stress / strain toward normal values, but when unloaded axially they do not recover their axial stress / strain (Jackson et al., 2005).

The uterus is a muscular organ that undergoes modest remodeling during normal menstruation, and marked remodeling during and early after pregnancy (Osol and Mandala, 2009). This organ is supplied by multiple arteries, including the uterine artery, which branches off the iliac artery. Uterine blood flow increases many-fold during pregnancy, then reduces back toward normal levels postpartum. Hormonal levels similarly change dramatically, with estrogen levels increasing during pregnancy, then reducing back toward normal levels postpartum. It is well known that estrogen affects vascular remodeling directly (Osol and Moore, 2014; Tarhouni et al., 2013), similar to effects of other circulating substances that change from the prenatal to postnatal circulation – for example, high levels of PGE2 in the fetal circulation that are lost postnatally, apparently contributing to closing of the ductus arteriosus (Yamashiro and Yanagisawa, 2020). The goal of this paper was to determine whether the expected dramatic pregnancy-induced remodeling of the uterine artery reverses fully postpartum. Toward this end, we quantified compositional and biomechanical changes of the uterine artery from late gestation to the early and later postpartum periods and assessed these changes relative to the geometry and properties prior to pregnancy as well as relative to the remodeling ascending aorta, which also experiences dramatic increases in blood flow during pregnancy.

METHODS

All methods, both experimental (Ferruzzi et al., 2013) and computational (Latorre and Humphrey, 2018a), have been validated previously, and thus are described only briefly here.

Animals. Studies were performed on 11 to 14 week old adult female C57BL/6J mice. At one of four prescribed times – before pregnancy, late gestation, early postpartum, and later postpartum – the mice were euthanized with an intraperitoneal injection of Beuthanasia-D and both the ascending aorta (an elastic artery) and a uterine artery (a muscular artery) were excised and prepared for *ex vivo* biomechanical testing.

Biaxial Testing and Quantification. Cannulated vessels were placed within a custom, computer-controlled device (Gleason et al., 2004) in a Hank's buffered physiological solution to focus on passive mechanical responses. Following a short equilibration period, the vessels were preconditioned mechanically via cyclic pressurization while held at their preferred (*in vivo*) value of axial stretch, λ_z^{iv}, then subjected to a series of seven biaxial protocols: group-specific cyclic pressurization protocols at specimen-specific values of λ_z^{iv} that were repeated at ±5% of this stretch, as well as group-specific axial stretching protocols at four group-specific values fixed luminal pressures. The associated passive pressure-diameter and axial force-length data were fit with a validated four-fiber family constitutive model via nonlinear regression of a data set that consisted of the final cycle of unloading data from all seven protocols. Using data during unloading reveals the elastic energy stored during deformation that would be available to work on the distending fluid during unloading. This "four-fiber family" constitutive relation has been validated independently (Schroeder et al., 2018) and includes eight model parameters within a Holzapfel-type nonlinear stored energy function W, namely

$$W\left(\mathrm{C}, \mathrm{M}^i\right) = \frac{c}{2}(I_\mathrm{C} - 3) + \sum_{i=1}^{4} \frac{c_1^i}{4c_2^i}\left\{\exp\left[c_2^i\left(IV_\mathrm{C}^i - 1\right)^2\right] - 1\right\}, \tag{1}$$

where c (kPa), c_1^i (kPa), and c_2^i (-) are model parameters. Here, $i = 1,2,3,4$ denote four predominant fiber family directions given by $\mathbf{M}^i = \left[0,\ \sin\alpha_0^i,\ \cos\alpha_0^i\right]$, with α_0^i denoting a fiber angle relative to the axial direction in the traction-free reference configuration: axial ($\alpha_0^1 = 0$), circumferential ($\alpha_0^2 = \pi/2$), and symmetric diagonal ($\alpha_0^{3,4} = \pm\alpha_0$). Note, too, that $I_\mathrm{C} = tr(\mathbf{C})$ and $IV_\mathrm{C}^i = \mathbf{M}^i \cdot \mathbf{C}\mathbf{M}^i$ are coordinate invariant measures of the finite deformation, with the right Cauchy-Green tensor $\mathbf{C} = \mathbf{F}^\mathrm{T}\mathbf{F}$ computed from the deformation gradient tensor $\mathbf{F} = \mathrm{diag}[\lambda_r, \lambda_\theta, \lambda_z]$, with $det\mathbf{F} = 1$ because of assumed incompressibility. Values of mean biaxial wall stress and material stiffness were computed from the stored energy function (Baek et al., 2007) and calculated at both individually measured values of blood pressure and at a common pressure.

Histology and Immunohistochemistry. Following biomechanical testing, specimens were unloaded and fixed overnight in 10% neutral buffered formalin, then stored in 70% ethanol at 4°C for histological examination. Fixed samples were dehydrated, embedded in paraffin, sectioned serially (5-μm thickness), and stained with Elastica Van Gieson (EVG) or Movat pentachrome (MOV). Detailed analyses were performed on three biomechanically representative vessels for each age group. Custom MATLAB scripts extracted layer-specific cross-sectional areas and calculated positively stained pixels and area fractions (AF). Histological images were acquired on an Olympus BX/51 microscope using an Olympus DP70 digital camera (CellSens Dimension) and a 20x magnification objective.

Computational modeling. Over the past twenty years, we have developed, refined, and used a constrained mixture model of arterial growth and remodeling (G&R) that has proven to be a reliable descriptor and predictor of diverse cases of vascular adaptation and disease progression (Humphrey, 2021). Briefly, this model accounts for individual natural (stress-free) configurations, deformations, material properties, and rates of turnover of different structurally significant constituents. We yet solve classical linear momentum balance in terms of the mixture Cauchy stress, which necessitates a constitutive relation for the stored energy function, which we assume follows a simple rule-of-mixtures relation (Humphrey and Rajagopal, 2002), $W_{\mathrm{R}} = \sum W_{\mathrm{R}}^{\alpha}$ at any G&R time s, where the constituent-specific strain energy per unit reference volume of mixture is

$$W_{\mathrm{R}}^{\alpha}(s) = \frac{\rho_{\mathrm{R}}^{\alpha}(0)Q^{\alpha}(s)}{\rho}\widehat{W}^{\alpha}\left(\mathbf{C}_{\mathrm{n}(0)}^{\alpha}(s)\right) + \int_{0}^{s}\frac{m_{\mathrm{R}}^{\alpha}(\tau)q^{\alpha}(s,\tau)}{\rho}\widehat{W}^{\alpha}\left(\mathbf{C}_{\mathrm{n}(\tau)}^{\alpha}(s)\right)\mathrm{d}\tau \qquad (2)$$

with $\rho = \rho_{\mathrm{R}}/J$ the mixture mass density (where $\rho_{\mathrm{R}} = \sum\rho_{\mathrm{R}}^{\alpha}$ and $J = \det\mathbf{F} > 0$), $m_{\mathrm{R}}^{\alpha}(\tau) > 0$ the true rate of referential mass density production, and $q^{\alpha}(s,\tau) \in [0,1]$ a survival function that accounts for that part of a constituent that persists at current G&R time s when deposited at prior time $\tau \in [0,s]$ (with $Q^{\alpha}(s) = q^{\alpha}(s,0)$). Moreover, $\widehat{W}^{\alpha}(\mathbf{C}_{\mathrm{n}(\tau)}^{\alpha}(s)) > 0$, with $\mathbf{C}_{\mathrm{n}(\tau)}^{\alpha}(s) = \mathbf{F}_{\mathrm{n}(\tau)}^{\alpha\mathrm{T}}(s)\mathbf{F}_{\mathrm{n}(\tau)}^{\alpha}(s)$, is the stored energy per unit volume of constituent α that depends on the deformation gradient $\mathbf{F}_{\mathrm{n}(\tau)}^{\alpha}(s) = \mathbf{F}(s)\mathbf{F}^{-1}(\tau)\mathbf{G}^{\alpha}(\tau)$ experienced by that constituent at current time s relative to its potentially evolving natural configuration $\mathrm{n}(\tau)$, with $\mathbf{G}^{\alpha}(\tau)$ the cell-mediated pre-stretch at the time of deposition $\tau \in [0,s]$.

Following prior work, we assume a neo-Hookean model for the elastin-dominated matrix and Fung-exponential models for collagen-dominated and smooth muscle-dominated constituents within the uterine artery. Motivated by prior work on immuno-mechano-mediated stimulation of cell and matrix turnover (Latorre and Humphrey, 2018a), we introduce a modified relation for hormono-mechano-mediated mass density production, namely

$$m_{\mathrm{R}}^{\alpha}(\tau) = k_{\mathrm{N}}^{\alpha}(\tau)\rho_{\mathrm{R}}^{\alpha}(\tau)\left(1 + \mathrm{K}_{\sigma}^{\alpha}\Delta\sigma - \mathrm{K}_{\tau_w}^{\alpha}\Delta\tau_w + \mathrm{K}_{e}^{\alpha}\Delta e\right) \qquad (3)$$

where $\Delta\sigma = (\sigma - \sigma_o)/\sigma_o$ and $\Delta\tau_w = (\tau_w - \tau_{wo})/\tau_{wo}$ represent deviations in mean pressure- and axial force-induced intramural stress (taken as the first invariant of the Cauchy stress) and flow-induced wall shear stress (taken from a steady state Poiseuille solution) from homeostatic values (σ_o and τ_{wo} are homeostatic scalar metrics), with $\mathrm{K}_{\sigma}^{\alpha} > 0$ and $\mathrm{K}_{\tau_w}^{\alpha} > 0$ constituent-specific gain-type parameters that define the sensitivity of the response to the stress deviation. Similarly, Δe represents changes in estrogen levels from baseline with $\mathrm{K}_{e}^{\alpha} > 0$ modulating the sensitivity of the response to these changes.

Finally, we let k_{N}^{α} denote evolving rate parameters within a generalized first-order kinetic decay for removal

$$q^{\alpha}(s,\tau) = \exp\left(-\int_{\tau}^{s} k_{\mathrm{N}}^{\alpha}(t)\,\mathrm{d}t\right). \tag{4}$$

with $k_{\mathrm{N}}^{\alpha} = k_o^{\alpha}(1 + \omega(\Delta\sigma)^2)$ increasing via (squared) deviations in intramural stress, with k_o^{α} baseline rate parameters and ω another gain-type parameter herein. Homeostasis requires balanced production and removal within unchanging mechanical states, hence $m_o^{\alpha} = \rho_o^{\alpha} k_o^{\alpha}$ while $\mathbf{F}_{\mathrm{n}(\tau)}^{\alpha}(s) = \mathbf{G}^{\alpha}(\tau)$.

Modeling Assumptions. Because of marked hormonal changes during and following pregnancy, we assumed that serum estrogen increases to a maximum value just before delivery, then decreases rapidly, which the model replicates as a prescribed input (see Supplemental Information). For the four-fiber-family model parameters to capture the measured biomechanical responses of the uterine artery, both original and evolved, we let the elastin material parameter evolve as well. The nonlinear regression required that this parameter approach 0 to fit the evolved data after delivery, consistent with changes in the shape of the P-d curves from an S-shape to largely exponential in this muscular artery.

Importantly, we used a full constrained mixture model (heredity integral based) for our primary simulations (Latorre and Humphrey, 2018a), but a mechanobiologically equilibrated model to determine baseline parameters (Latorre and Humphrey, 2018b). For more details, please see the original papers.

RESULTS

Figure 1 shows the systemic arterial tree from the ascending thoracic aorta (ATA) to a uterine artery (UtA) that branches off an iliac artery. Data were collected for both of these vessels from 14-wk old nulliparous (not previously pregnant) nongravid (not currently pregnant) female mice (NG, n=5), ~11-wk old antepartum mice at E18.5 (AP, n=4-5), ~11-wk old early postpartum mice 2 days after delivery (EPP, n=4-5) and 14-wk old later postpartum mice 21 days after delivery (LPP, n=5), noting that the pups are typically weaned by 3 weeks of age and that a female mouse can become pregnant soon after delivery and have a second litter within ~25 days after the first delivery.

Uterine arteries experience marked compositional and geometric remodeling during pregnancy that are largely reversed postpartum. Figure 1A-D shows representative histological sections for the UtA at each of the four study times, which reveal characteristic features of a muscular artery – a smooth muscle cell-rich medial layer delimited by internal and external elastic laminae and supported by a relatively thick collagen-rich adventitial layer. Associated quantification revealed no change in the medial area fraction of elastin at any of the four study times (panel E), but a marked increase in medial cytoplasm (i.e., smooth muscle cells) antepartum that was largely, though not completely, resolved postpartum (panel F). Nevertheless, there was no difference, on average, in total medial cross-sectional area ante- or post-partum (panel G) but a significant increase in adventitial cross-sectional area antepartum that was resolved postpartum (panel H).

Compositional and geometric changes affect material and structural properties. Figures 2 and 3 show multiple biomechanical metrics for the UtA at each of the four study times, including circumferential and axial. Pressure-diameter responses showed a marked rightward shift antepartum that was largely reversed postpartum in the physiologic pressure range though not at low pressures (Figure 2A). Focusing on physiologically relevant values, inner radius was necessarily increased significantly antepartum but largely restored postpartum (Figure 2B) while pressurized wall thickness differed only postpartum (Figure 2D). Importantly, there was a significant increase in circumferential material stiffness antepartum that was not reversed postpartum (Figure 1D) despite a full postpartum reversal of the antepartum increase in the mean circumferential wall stress (Figure 1E).

Axial properties for the UtA also differed across the four study times, though less dramatically and less consistently than circumferential properties. Modest differences in overall axial force-stretch responses emerged both antepartum and early postpartum, but the late postpartum behavior was yet similar to control, particularly at physiologic loads (Figure 2A). The UtA lengthened during pregnancy, but returned to a near normal length postpartum (Figure 2B); these changes were reflected in modest changes in the inferred *in vivo* value of axial stretch (Figure 2C), that is, the value of axial stretch at which axial force changes little during cyclic pressurization (Humphrey et al., 2009). In contrast to circumferential changes, there were modest changes in axial material stiffness (Figure 2D) and mean axial wall stress (Figure 2E). See Supplemental Figure S1 for associated biaxial Cauchy stress – stretch behaviors.

The ascending aorta remodels during and after pregnancy, largely recovering original properties. The ATA necessarily experiences the entire increase in cardiac output that occurs in pregnancy. Supplemental Figure S2 shows overall pressure-diameter and axial force-stretch responses by the ATA at the four study times: before, during, and two times following pregnancy. Figure 4 contrasts directly two

key biomechanical metrics for an elastic artery – elastic energy storage capability and calculated pulse wave velocity, a measure of structural stiffness – for the ATA and UtA at each of the four study times. As it can be seen, the elastic energy storage increased significantly in the UtA antepartum, but then assumed values lower than control in the postpartum period. By contrast, the ATA showed a mild increase in energy storage in pregnancy that decreased toward normal following delivery. The calculated pulse wave velocity also increased antepartum in the UtA but remained elevated postpartum whereas values in the ATA did not differ much during or following pregnancy. Additional comparisons between the remodeling of these two vessels (ATA – an elastic artery, and UtA – a muscular artery) are found in Supplemental Table S1, which shows further that UtA remodeling was generally greater and less reversible, at least over the three-week postpartum period.

A computational G&R model captures the complex evolution of the uterine artery. Computational G&R models can provide additional insight into progressive changes in composition, geometry, and properties and they can be used to generate and test hypotheses. Figure 5A,B shows simulated results for pressure-inner radius and axial force-stretch behaviors under normal *in vivo* conditions both antepartum and postpartum relative to non-pregnant control (NG). As it can be seen, the model captured qualitatively and quantitatively (with arrows showing a rightward shift followed by a leftward recovery) the observed pressure-diameter behaviors (Figure 2A) given the assumption of normotension with increased and then decreased blood flow- and estrogen-induced G&R. This result was achieved only by including two additional modeling assumptions: (i) compromising the mechanical functionality of the amorphous matrix in the model, which appears consistent with the permanent postpartum changes in the low-pressure structural response (cf. Figure 2A) and the reduced energy storage (cf. Figure 4A), and (ii) dramatically decreasing the half-life of the collagen, which appears consistent with a rapid turnover that likely gave rise to the marked thickening then thinning of the adventitia (cf. Figure 1H). The prediction of the axial response was less good, though it qualitatively described some of the main features as well (cf. Figure 3A). The computational model similarly captured some of the material behaviors – biaxial Cauchy stress-stretch – reasonably well (Figure S3).

Given these results, we then simulated two cases that were not explored experimentally but are nevertheless important clinically. First, we simulated the case of normal changes in blood flow and estrogen levels, but with elevated blood pressures during pregnancy (Figure 5C,D), which is relevant to fetal growth restriction. As it can be seen, the simulations suggested that superposition of hypertension on normal increases and then decreases in flow and estrogen may result in less favorable remodeling of the UtA. That is, hypertension was predicted to restrict the dilation of the UtA during pregnancy but to

lead to a larger remodeled caliber after delivery. Second, we simulated the case of normal changes in blood flow during pregnancy in the absence of prescribed changes in estrogen levels. Importantly, the model predicted that the normal (but otherwise dramatic) increase in flow alone would lead the UtA to grow uncontrollably in contrast to what one could expect (ovariectomizing rats suppresses remodeling in resistance arteries exposed to high flow; Tarhouni et al., 2013). Therefore, noting that endothelial NO is a key modulator of arterial G&R, being stimulated by a variety of factors, particularly shear stress but also estrogen (Osol and Moore, 2014), we repeated the simulation with a reduced gain $\mathrm{K}_{\tau_w}^{\alpha}$ for the shear stress stimulus in Eq. (3). Interestingly, a stable response, with nearly suppressed remodeling, is predicted for the UtA exposed to high flow conditions in this case, suggesting that a deficiency in estrogen may reduce the sensitivity of the response to the shear-stress deviation (Figure 5E,F). These results are generally consistent with observations from the literature (Tarhouni et al., 2013), suggesting that estrogen plays a primary, guiding role in the expansive, high flow-mediated remodeling during pregnancy.

DISCUSSION

Pregnancy associates with dramatic changes in the maternal circulation, including decreases in total peripheral resistance and increases in cardiac output that tend to be restored toward normal values within a few weeks postpartum. In particular, cardiac output increases by as much as 40-50% in humans during singleton pregnancy and up to an additional 15% in a twin pregnancy (Sanghavi and Rutherford, 2014). Even more dramatic are hemodynamic changes in the uterine artery. Mouse models have become widely used in the study of utero-placental and umbilico-placental hemodynamics given the short gestational period (~20 days) and ease of longitudinal study. Peak flow velocity in the uterine artery (UtA) has been reported to increase nearly linearly throughout gestation in the mouse, reaching a 2.5-fold increase in late gestation (59 cm/s at E18.5 relative to 23 cm/s prior to pregnancy), a progressive increase that is mirrored by a progressive decrease in vascular resistance (Mu and Adamson, 2006). Mechano-responsive arterial enlargement to increases in flow generally associate with increased eNOS production (Rudic et al., 1998), hence it is not surprising that uterine artery remodeling is compromised in eNOS knockout mice (Kulandavelu et al., 2012). Vascular changes antepartum and postpartum are influenced by many factors, however, including dramatic transient changes in both the hemodynamics and circulating hormones, especially estrogen (Pastore et al., 2012). Complicating the understanding of these different contributors is the observation that estradiol17β-induced increases in uterine blood flow are attenuated by eNOS antagonism (L-nitroarginine methyl ester), suggesting that estrogen-induced changes are also mediated by nitric oxide (van Buren et al., 1992). Computational models can, at times, help to delineate

separate, synergistic, or antagonistic effects. The two goals of this study, therefore, were to collect novel biomechanical data on the microstructural and biomechanical remodeling of the uterine artery antepartum and postpartum and to use these data to build a computational growth and remodeling model than could help to delineate the myriad contributions to the observed remodeling.

Whereas many prior studies have measured changes in uterine artery flow and associated vascular caliber throughout gestation and early postpartum (e.g., Mu and Adamson, 2006; Khankin et al., 2021), we are not aware of any prior study of temporal changes in the associated arterial microstructure and mechanical properties. Changes in the ascending thoracic aorta (ATA, an elastic artery) served herein as a relevant comparator for changes in the uterine artery (UtA, a special muscular artery). The inner radius of the UtA increased a dramatic 1.83 fold at E18.5 (relative to never-pregnant control), whereas the inner radius of the ATA increased a much more modest 1.02 fold, suggesting particularly dramatic increases in flow to the uterus during pregnancy. Based on an *in vivo* ligation model, it has been suggested that at least perturbations in uterine flow result in a mechano-regulated restoration of wall shear stress (Khankin et al., 2021). Recalling the aforementioned mechanobiological rule for such mechano-adaptation of luminal radius ($a \rightarrow \varepsilon^{1/3} a_o$), the measured 1.83-fold increase in UtA luminal radius, from 86 μm to 157 μm, suggests a 6-fold increase in volumetric flow, which, based on reported mean UtA velocities (~2.5; Mu and Adamson, 2006), appears to be of the right order of magnitude (i.e., $\sim 2.5 \cdot 1.83^2 = 8.59$, which is the maximal flow rate, at E18.5, that we used for our simulations). Mechano-adaptation of wall thickness ($h/h_o \rightarrow \varepsilon^{1/3}\gamma$) would require a much greater thickening ratio than the measured 20μm/21μm ~ 1, hence the elevated, far from adapted, circumferential stress measured at E18.5 (from 22 kPa to 42 kPa). Noting the rapid transient changes in hemodynamics, which the arterial wall tries to accommodate, plus the presence of circulating hormones, which may induce a maladaptive response, it is not surprising that a full mechano-adaptation is not yet achieved within the short period prior to late gestation in the mouse.

We modified a validated computational framework for vascular G&R to simulate the time course of changes in UtA geometry, composition, and properties. Use of such a model is consistent, of course, with biological studies that pregnancy related remodeling of the uterine circulation involves cell and matrix turnover as well as matrix reorganization in response to dramatic increases in blood flow and hormonal levels (Osol and Mandala, 2009). Noting the key role of estrogens in the long-term blood flow-mediated structural remodeling in resistance arteries (Tarhouni et al., 2013) and that “pregnancy-induced increases in circulating estrogen may not only facilitate uterine vascular remodeling but also amplify arterial circumferential growth in response to increased shear stress in upstream vessels” (Osol and Moore, 2014), we let estrogen directly stimulate G&R by extending a mechano-mediated stimulus

function for mass production (Humphrey, 2021) to include an additional term directly proportional to the changes in estrogen levels (i.e., $\mathrm{K}_e^\alpha \Delta e$ in Eq. (3)). Such an extended hormono-mechano-mediated relation for mass production parallels that of our prior work on immuno-mechano-mediated stimulation of cell and matrix turnover (Latorre and Humphrey, 2018a). Note that, with the model constructed in this way, $\Delta e > 0$ suggests a prioritization of estrogen-mediated remodeling over the pure mechano-mediated remodeling (because $\Delta e > 0$ prevents $\Delta\sigma$ and/or $\Delta\tau_w$ from approaching 0 in mechanobiological equilibrium, i.e., $m_{\mathrm{R}}^\alpha = k_{\mathrm{N}}^\alpha \rho_{\mathrm{R}}^\alpha$ in Eq. (3)), hence leading to a mechanical maladaptation, with the flow-induced shear stress likely remaining close to normal as a result of the increase in inner radius (Khankin et al., 2021), but not so the elevated circumferential stress as a result of a lack of thickening (Figure 2).

Interestingly, as in prior G&R studies, we needed to modify the stiffness of the newly produced constituents in order to fit the biomechanical data. We used estrogen content to drive the evolution of parameters in Eq. (1) within the deposition time-dependent integral in Eq. (2). In addition, we found that the elastin modulus needed to evolve (eventually vanishing) to fit the postpartum low-pressure structural response (Figure 2A), which also supports the reduced energy storage after delivery (Figure 4A). Of course, elastin plays a lesser role in muscular arteries than in elastic arteries, which have been the focus of much of our recent G&R work (Humphrey, 2021). The need for all of these model parameters to evolve (leading to the shifts and changes in the shape of the predicted biaxial responses in Figure 5), which was critical to describing the response throughout gestation and recovery, suggests theoretically and computationally that pregnancy-induced remodeling of the UtA does not reverse fully within three weeks postpartum during which the hemodynamic perturbation reverses (see, in particular, Figures 2 and 3). Finally, as in prior work (Latorre and Humphrey, 2018a; Weiss et al., 2021), we needed to accelerate the turnover rate for both smooth muscle and collagen, which seems consistent with the need for the arterial wall to rapidly accommodate the marked increase in blood flow required by the uterus, hence suggesting an important role of rates of matrix turnover in dictating arterial circumferential growth during pregnancy.

Taken together, these results suggest that pregnancy related changes in estrogen levels dominate and guide the rapid UtA remodeling antepartum and recovery postpartum under dramatic changes in blood flow, with hypertension likely compromising postpartum recovery.

CONFLICT OF INTERST

The authors declare not conflicts of interest, financial or otherwise.

REFERENCES

Baek S, Gleason RL, Rajagopal KR, Humphrey JD (2007) Theory of small on large: Potential utility in computations of fluid-solid interactions in arteries. Comp Meth Applied Mech Engr 196: 3070-3078.

Gleason RL, Gray SP, Wilson E, Humphrey JD (2004) A multiaxial computer-controlled organ culture and biomechanical device for mouse carotid arteries. ASME J Biomech Engr 126: 787-795.

Ferruzzi J, Bersi MR, Humphrey JD (2013) Biomechanical phenotyping of central arteries in health and disease: Advantages of and methods for murine models. Annl Biomed Engr 41: 1311-1130.

Humphrey JD, Rajagopal KR (2002) A constrained mixture model for growth and remodeling of soft tissues. Math Model Meth Appl Sci 12: 407-430.

Humphrey JD (2008) Mechanisms of arterial remodeling in hypertension: Coupled roles of wall shear and intramural stress. Hypertension 52: 195-200.

Humphrey JD, Eberth JF, Dye WW, Gleason RL (2009) Fundamental role of axial stress in compensatory adaptations by arteries. J Biomech 42: 1-8.

Humphrey JD (2021) Constrained mixture models of tissue growth and remodeling – Twenty years after. J Elasticity 145:49-75.

Jackson ZS, Dajnowiec D, Gotlieb AI, Langille BL (2005) Partial off-loading of longitudinal tension induces arterial tortuosity. Arterioscler Thromb Vasc Biol. 25(5):957-62.

Khankin EV, Ko NL, Mandala M, Karumanchi SA, Osol G (2021) Normalization of wall shear stress as a physiological mechanism for regulating material uterine artery expansive remodeling during pregnancy. FASEB BioAdvances 3: 702-708.

Kulandavelu S, Whiteley KJ, Qu D, Mu J, Bainbridge SA, Adamson SL (2012) Endothelial nitric oxide synthase deficiency reduces uterine blood flow, spiral artery elongation, and placental oxygenation in pregnant mice. Hypertension 60: 231-238.

Latorre M, Humphrey JD (2018a) Modeling mechano-driven and immuno-mediated aortic maladaptation in hypertension Biomech Model Mechanobiol 17: 1497-1511.

Latorre M, Humphrey JD (2018b) A mechanobiologically equilibrated constrained mixture model for growth and remodeling of soft tissues. Zeitschrift fur Angewandte Mathematik und Mechanik (ZAMM) 98: 2048-2071.

Mu J, Adamson SL (2006) Developmental changes in hemodynamics of uterine artery, utero- and umbilico-placental, and vitelline circulations in mouse throughout gestation. Am J Physiol 291: H1421-H1428.

Osol G, Mandala M (2009) Maternal uterine vascular remodeling during pregnancy. Physiology 24: 58-71.

Osol G, Moore LG (2014) Maternal uterine vascular remodeling during pregnancy. Microcirculation 21: 38-47.

Pastore MB, Jobe SO, Ramadoss J, Maqness RR (2012) Estrogen receptor-α and estrogen receptor-β in the uterine vascular endothelium during pregnancy: Functional implications for regulating uterine blood flow. Semin Reprod Med 30: 46-61.

Rudic RD, Shesely EG, Maeda N, Smithies O, Segal SS, Sessa WC (1998) Direct evidence for the importance of endothelium-derived nitric oxide in vascular remodeling. J Clin Invest 101:731-736.

Sanghavi M, Rutherford JD (2014) Cardiovascular physiology of pregnancy. Circulation 130: 1003-1008.Tarhouni K, Guihot AL, Freidja ML, Toutain B, Henrion B, Baufreton C, Pinaud F, Procaccio V, Grimaud L, Ayer A, Loufrani L (2013) Key role of estrogens and endothelial estrogen receptor α in blood flow–mediated remodeling of resistance arteries. Arterioscler Thromb Vasc Biol 33: 605-611.

Schroeder F, Polzer S, Slazansky M, Man V, Skacel P (2018) Predictive capabilities of various constitutive models for arterial tissue. J Mech Behav Biomed Mater 78: 369-380.

Tarhouni K, Guihot AL, Freidja ML, Toutain B, Henrion B, Baufreton C, Pinaud F, Procaccio V, Grimaud L, Ayer A, Loufrani L, Lenfant F, Arnal JF, Henrion D (2013) Key role of estrogens and endothelial estrogen receptor α in blood flow-mediated remodeling of resistance arteries. Arterioscler Thromb Vasc Biol. 33:605-611.

Van Buren GA, Yang D-S, Clark KE (1992) Estrogen-induced uterine vasodilatation is antagonized by L-nitroargine metyl ester, and inhibitor of nitric oxide synthesis. Am J Obstet Gynecol 167: 828-833.

Weiss D, Latorre M, Rego B, Cavinato C, Berman AG, Goergen CJ, Humphrey JD (2021) Biomechanical consequences of compromised elastic fiber integrity and matrix cross-linking on abdominal aortic aneurysmal enlargement. Acta Biomat 134:422-434.

Wolinsky H (1971) Effects of hypertension and its reversal on the thoracic aorta of male and female rats. Morphological and chemical studies. Circ Res. 28:622-637.

Wolinsky H (1972) Effects of estrogen and progestogen treatment on the response of the aorta of male rats to hypertension. Morphological and chemical studies. Circ Res. 30:341-349.

Yamashiro Y, Yanagisawa H (2020) The molecular mechanism of mechanotransduction in vascular homeostasis and disease. Clin Sci (Lond) 134:2399-2418.

FIGURES

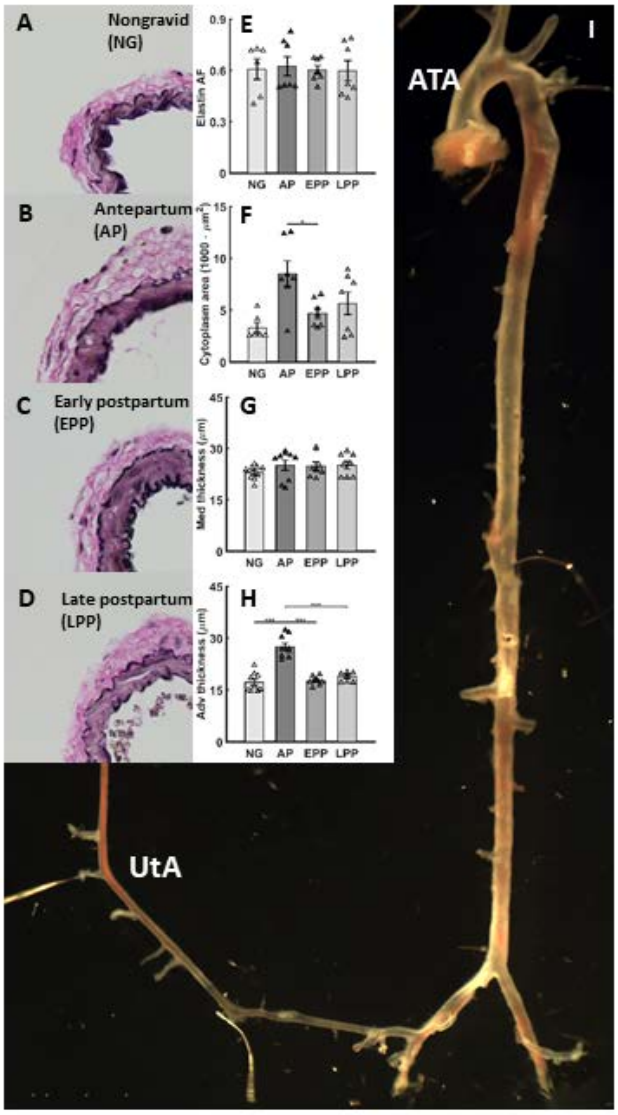

Figure 1. A-D: EVG staining of uterine arteries (UtA) from 14-wk old nulliparous nongravid female mice (NG, open symbols), 11-wk old antepartum pregnant mice at E18.5 (AP, black symbols), 11-wk old early postpartum mice 2 days after delivery (EPP, dark-gray symbols), and 14-wk old later postpartum mice 21 days after delivery (LPP, light-gray symbols). E,F: Histological quantification revealed no significant differences in elastin area fraction (AF) or medial wall thickness during and after pregnancy. G,H: There was, however, a significant increase in adventitial thickness and cytoplasm area antepartum, which was resolved by early postpartum. I: Illustrative image of an excised arterial tree from the ascending thoracic aorta (ATA) to uterine arteries (UtA) branching off the iliac artery.

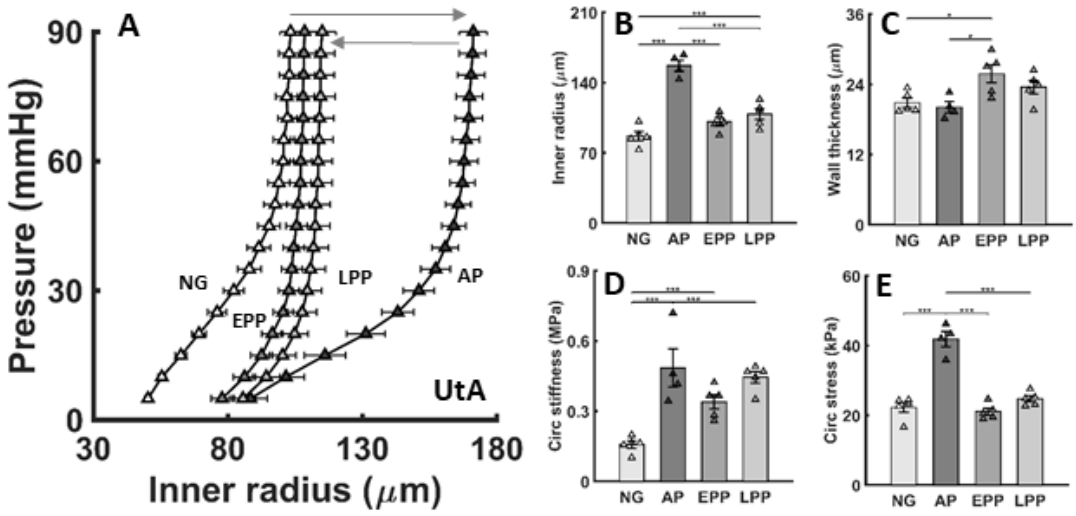

Figure 2. Circumferential properties of uterine arteries (UtA, triangle) from 14-wk old nulliparous nongravid female mice (NG, open symbols), 11-wk old antepartum pregnant mice at E18.5 (AP, black symbols), ~11-wk old early postpartum mice 2 days after delivery (EPP, dark-gray symbols), and 14-wk old later postpartum mice 21 days after delivery (LPP, light-gray symbols). A: Significant right-ward shift of the pressure-inner radius relationship was found AP compared to NG, which was resolved by EPP for pressure > 40mmHg. No significant difference was found between the pressure-inner radius relationships at EPP and LPP. B: The loaded inner radius increased significantly during pregnancy (AP), then decreased rapidly after delivery (EPP) nearly recovering the NG lumen size at LPP. C: Loaded wall thickness was not significantly different at AP but was increased at EPP, though less so at LPP. D,E: Circumferential material stiffness and wall stress increased significantly at AP, with stiffness remaining elevated at EPP and LPP while wall stress was restored to NG values at these times. All metrics in panels B-E were analyzed at 40 mmHg.

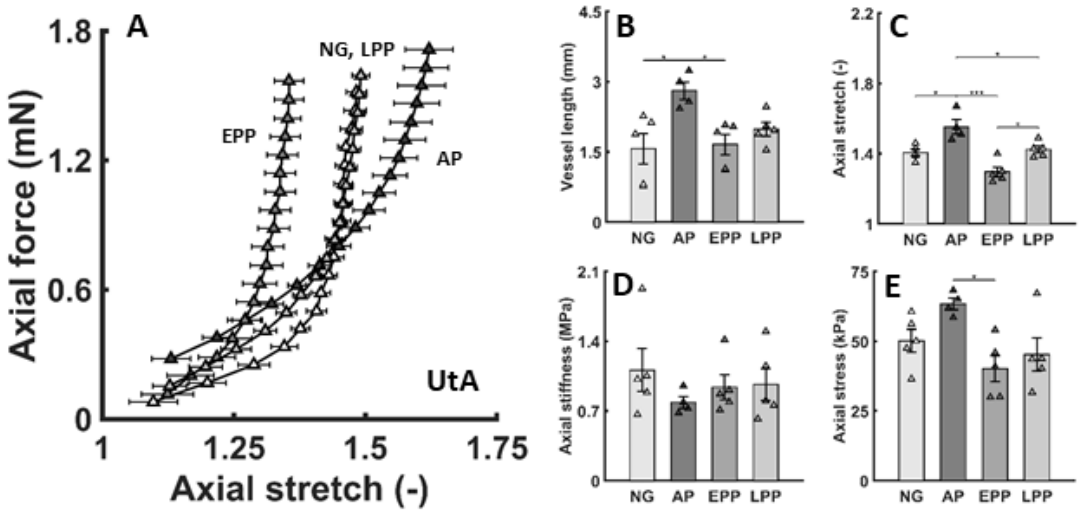

Figure 3. Similar to Figure 2, except for axial properties of uterine arteries (UtA, triangle). A: Axial force – stretch relationships were dramatically different during AP and EPP but were restored by LPP. B,C: Loaded vessel length and axial stretch both increased at AP but were restored to NG values by EPP. D,E: Axial stiffness did not change significantly though axial stress increased, then decreased back to values similar to NG.

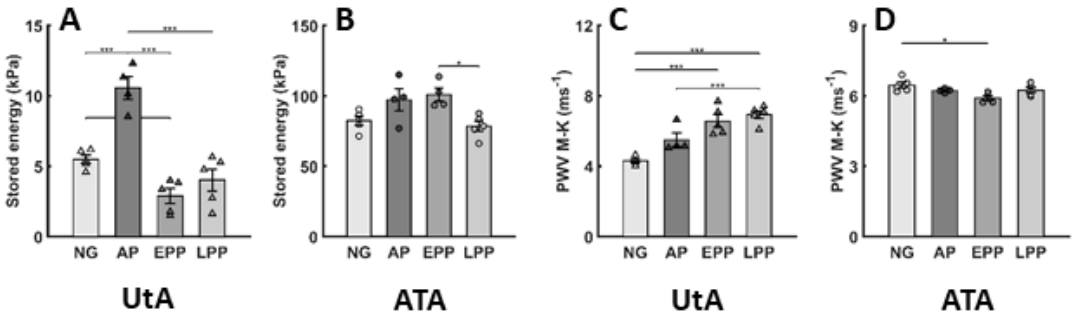

Figure 4. Direct comparison of remodeling of the uterine artery (UtA) and ascending thoracic aorta (ATA). A,B: Stored (elastic) energy capacity was significantly increased at AP but restored by LPP in the UtA whereas a trend of increase was observed at AP and EPP in the ATA, with values returning to normal by LPP. C,D: The local pulse wave velocity (PWV), calculated using the Moens-Korteweg (M-K) equation, increased significantly in the UtA during EPP and LPP whereas there was a mild decrease in the ATA at EPP that reversed at LPP toward normal.

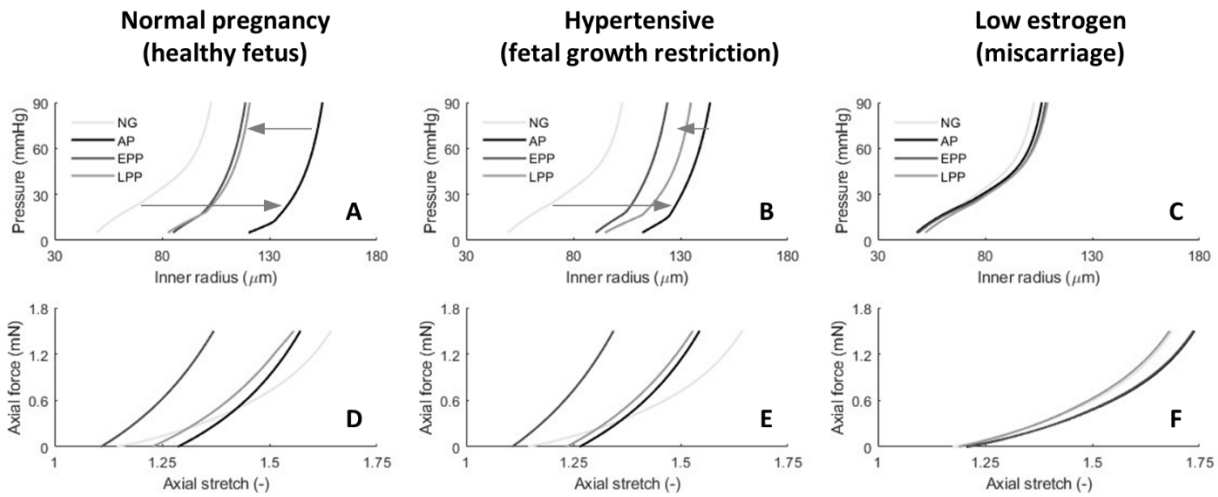

Figure 5. Computational model predictions of evolving passive biaxial structural responses (first row: distending pressure-inner radius behavior at individual values of *in vivo* axial stretch; second row: applied axial force-stretch behavior at a fixed luminal pressure of 40 mmHg) for uterine arteries (UtA) from 14-wk old nulliparous nongravid female mice (NG, lightest-grey lines), 11-wk old antepartum pregnant mice at E18.5 (AP, black), 11-wk old early postpartum mice 2 days after delivery (EPP, dark-gray), and 14-wk old late postpartum mice 21 days after delivery (LPP, light-gray) under actual (left panels; high blood flow-induced G&R, with estrogen; cf. Figs. 2A and 3E) and either simulated hypertension (central; high blood flow- and pressure-induced G&R, with estrogen) or simulated low estrogen (right; high blood flow-induced G&R, without estrogen) conditions. Model parameters were determined from normal NG and EPP data only, assumed as mechanobiologically equilibrated states, whereas all biaxial responses were computed (i.e., predicted) by allowing the full G&R model to evolve from NG (initial) to LPP (final) under prescribed, case-specific, changes (gradual increase from NG to AP followed by a rapid decrease to EPP and then sustained) in blood flow, pressure or estrogen levels. Note that hypertension restricts the dilation of the UtA during pregnancy but leads to a larger remodeled caliber after delivery; by contrast, simulated estrogen-induced G&R is dominant relative to flow- (compare left to right panels) and pressure- (compare left to central panels) induced G&R.

Supplemental Information

Remodeling of the Uterine Artery During and Early After Pregnancy in the Mouse

Sae-Il Murtada[1,*], Marcos Latorre[2,*], Jay D. Humphrey[1,3]

[1]Department of Biomedical Engineering
Yale University, New Haven, CT, USA

[2]Center for Research and Innovation in Bioengineering
Universitat Politècnica de València, València, Spain

[3]Vascular Biology and Therapeutics Program
Yale School of Medicine, New Haven, CT, USA

[*]These authors contributed equally

Supplemental Figures

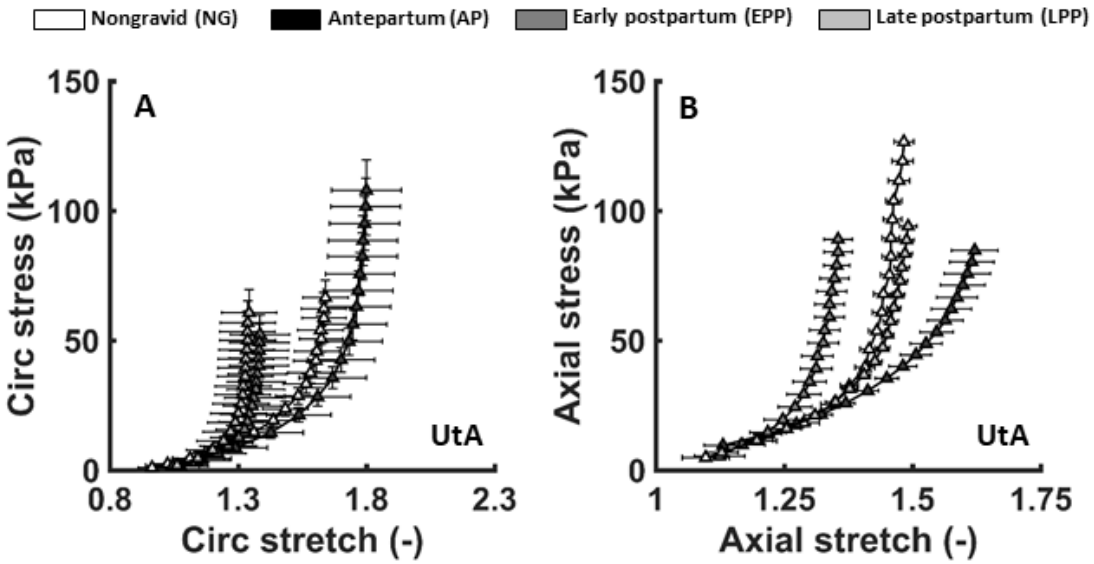

Figure S1. Related to Figures 2 and 3 for the uterine artery (UtA), but for the biaxial Cauchy stress-stretch behaviors at all four study times: 14-wk old nulliparous nongravid female mice (NG, lightest-grey lines), 11-wk old antepartum pregnant mice at E18.5 (AP, black), 11-wk old early postpartum mice 2 days after delivery (EPP, dark-gray), and 14-wk old late postpartum mice 21 days after delivery (LPP, light-gray). See also symbols at the top.

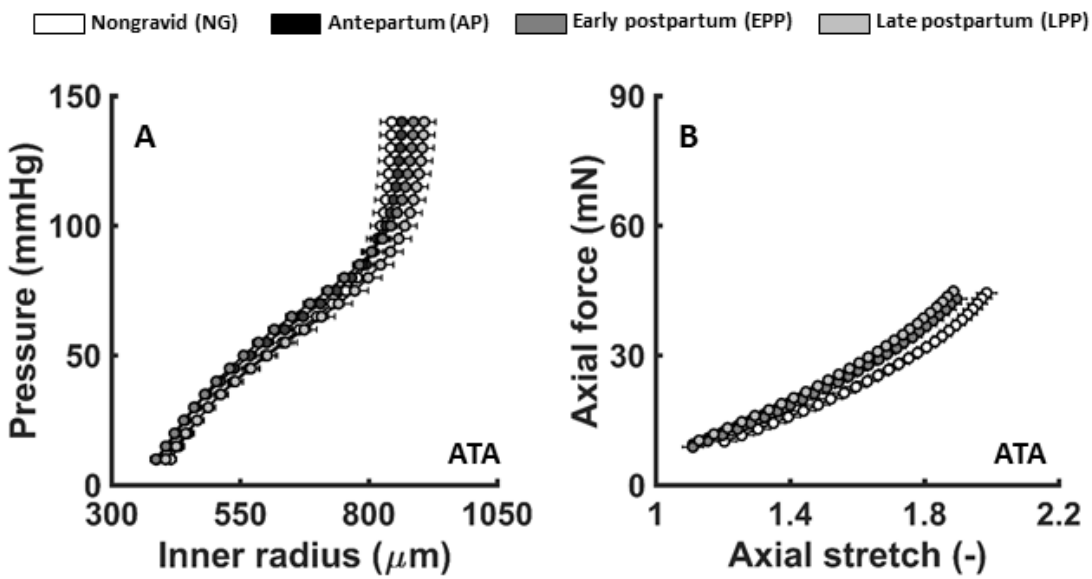

Figure S2. Similar to Figures 2A and 3A except for the ascending thoracic aorta (ATA), again for all four study times: 14-wk old nulliparous nongravid female mice (NG, lightest-grey lines), 11-wk old antepartum pregnant mice at E18.5 (AP, black), 11-wk old early postpartum mice 2 days after delivery (EPP, dark-gray), and 14-wk old late postpartum mice 21 days after delivery (LPP, light-gray). See also symbols at the top.

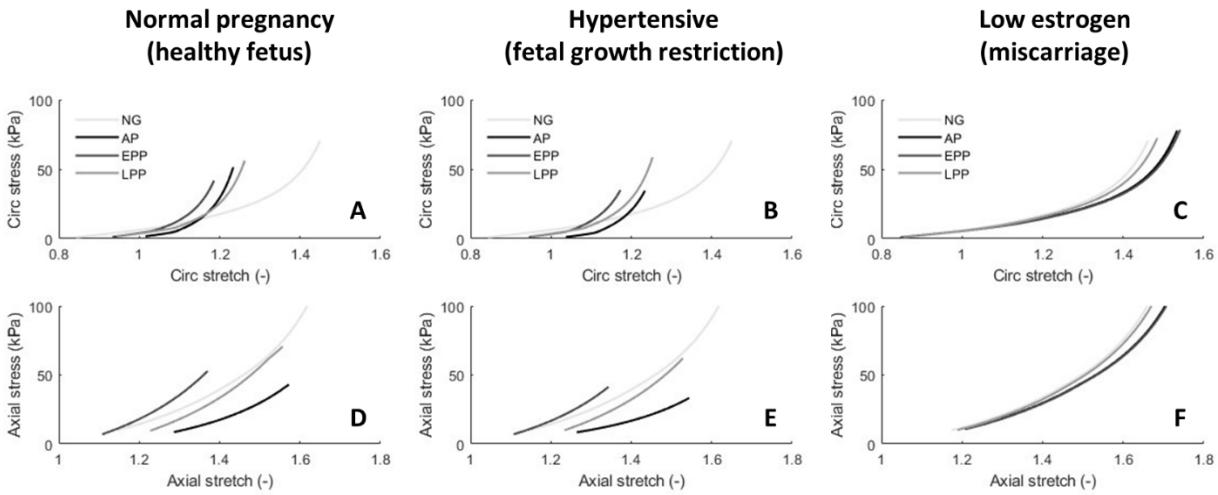

Figure S3. Similar to Figure 5 but for additional biomechanical metrics (panels A-F). Computational model predictions of evolving passive biaxial mechanical responses for uterine arteries (UtA) from 14-wk old nulliparous nongravid female mice (NG, lightest-grey lines), 11-wk old antepartum pregnant mice at E18.5 (AP, black), 11-wk old early postpartum mice - 2 days after delivery (EPP, dark-gray), and 14-wk old late postpartum mice - 21 days after delivery (LPP, light-gray) under actual (left panels; high blood flow-induced G&R, with estrogen; cf. Figs. 2A and 3E) or either simulated/modified hypertension (central; high blood flow- and pressure-induced G&R, with estrogen) or low estrogen (right; high blood flow-induced G&R, without estrogen) conditions.

Supplemental Table

Table S1. Geometric and mechanical metrics for the uterine artery (UtA) and ascending thoracic aorta (ATA) at all four study times, before and after pregnancy.

	Uterine artery (UtA)				Ascending thoracic aorta (ATA)			
	Cntl	Ante-partum E18.5	Post-partum 2 days	Post-partum 21 days	Cntl	Ante-partum E18.5	Post-partum 2 days	Post-partum 21 days
	n = 5	n = 4	n = 5	n = 5	n = 5	n = 4	n = 4	n = 5
Unloaded dimensions								
Outer Diameter (μm)	179 ± 5	253 ± 13	218 ± 10	231 ± 10	1152 ± 13	1084 ± 9	1095 ± 23	1157 ± 22
Wall Thickness (μm)	41 ± 0.9	52 ± 1.0	43 ± 1.5	43 ± 2.0	124 ± 3.6	111 ± 2.0	113 ± 4.3	138 ± 3.6
Loaded dimensions	**P = 40**	**P = 40**	**P = 40**	**P = 40**	**P = 100**	**P = 100**	**P = 100**	**P = 100**
Outer Diameter (μm)	215 ± 8.9	354 ± 11.6	253 ± 10.4	264 ± 12.7	1677 ± 44.5	1694 ± 37.8	1686 ± 25.4	1778 ± 46.4
Wall Thickness (μm)	21 ± 0.8	20 ± 0.9	26 ± 1.5	24 ± 1.1	41 ± 1.3	36 ± 1.4	37 ± 0.9	45 ± 1.7
Inner Radius (μm)	86 ± 4.5	157 ± 5.6	101 ± 4.0	109 ± 5.5	797 ± 22.3	811 ± 20.2	806 ± 12.1	844 ± 23.6
In vivo Axial Stretch (λ_{iv})	1.41 ± 0.02	1.55 ± 0.04	1.30 ± 0.03	1.42 ± 0.02	1.90 ± 0.02	1.80 ± 0.04	1.84 ± 0.06	1.81 ± 0.02
In vivo Circumferential Stretch (λ_{ii})	1.41 ± 0.05	1.67 ± 0.08	1.31 ± 0.05	1.28 ± 0.04	1.59 ± 0.03	1.70 ± 0.03	1.68 ± 0.02	1.70 ± 0.04
Systolic Cauchy Stresses (kPa)								
Circumferential, $\sigma_{\theta\theta}$	22 ± 1.4	42 ± 2.2	21 ± 1.0	25 ± 0.9	259 ± 11.3	299 ± 18.4	294 ± 4.8	251 ± 12.9
Axial, σ_{ZZ}	50 ± 4.1	63 ± 2.1	40 ± 4.7	45 ± 5.9	267 ± 11.0	296 ± 16.1	300 ± 9.9	237 ± 9.1
Systolic Linearized Stiffness (MPa)								
Circumferential, $\mathfrak{C}^{c}_{\theta\theta\theta\theta}$	0.16 ± 0.02	0.48 ± 0.08	0.34 ± 0.03	0.45 ± 0.02	1.62 ± 0.11	1.74 ± 0.11	1.54 ± 0.07	1.48 ± 0.12
Axial, $\mathfrak{C}_{ZZZZ}$	1.11 ± 0.22	0.79 ± 0.06	0.94 ± 0.12	0.97 ± 0.16	1.24 ± 0.06	1.39 ± 0.04	1.37 ± 0.07	1.13 ± 0.04
PWV B-H	3.54 ± 0.05	3.84 ± 0.26	6.80 ± 0.31	7.90 ± 0.79	5.60 ± 0.17	4.85 ± 0.13	4.35 ± 0.12	4.86 ± 0.15
Systolic Stored Energy (kPa)	5 ± 0.3	11 ± 0.8	3 ± 0.5	4 ± 0.8	82 ± 3.3	97 ± 7.8	101 ± 4.8	78 ± 3.6